https://doi.org/10.5194/egusphere-2025-764
Preprint. Discussion started: 17 March 2025

The Antarctic Ice Sheet sliding law inferred from seismic observations

Kevin Hank[1], Robert J. Arthern[1], C. Rosie Williams[1], Alex M. Brisbourne[1], Andrew M. Smith[1], James A. Smith[1], Anna Wåhlin[2], and Sridhar Anandakrishnan[3]

[1]Natural Environment Research Council, British Antarctic Survey, High Cross, Madingley Road, Cambridge, CB3 0ET, United Kingdom
[2]Department of Marine Sciences, University of Gothenburg, Gothenburg, Sweden
[3]Department of Geoscience, Pennsylvania State University, University Park, Pennsylvania, 16802, USA
*kevhan@bas.ac.uk

Correspondence: Kevin Hank (kevhan@bas.ac.uk)

Abstract. The response of the Antarctic ice sheet to climate change and its contribution to sea level under different emission scenarios are subject to large uncertainties. A key uncertainty is the slipperiness at the ice sheet base and how it is parameterized in glaciological projections. Alternative formulations of the sliding law exist, but very limited access to the ice base makes it difficult to select among them. Here, we use satellite observations of ice flow, inverse methods, and a theory of acoustic propagation in granular material to relate the effective pressure, which is a key control of basal sliding, to seismic observations recovered from Antarctica. Together with independent estimates of grain diameter and porosity from sediment cores, this enables a comparison of basal sliding laws within a Bayesian framework. The presented direct link between seismic observations and sliding law parameters can be readily applied to any acoustic impedance data collected in a glacial environment. For rapidly sliding tributaries of Pine Island Glacier, these calculations provide support for a Coulomb-type sliding law and widespread low effective pressures.

1 Introduction

Large uncertainties accompany sea level rise projections for the 21st century. Relative to 1900, the estimates vary between ~ 50 and > 100 cm (IPCC Core Writing Team, H. Lee and J. Romero (eds.), 2023). This uncertainty hampers the formulation of adaptation strategies. A key source of uncertainty is the slipperiness of the bed beneath regions of fast-flowing ice streams (Ritz et al., 2015; Brondex et al., 2017), particularly in the Amundsen Sea Embayment (e.g., Nias et al., 2018; Joughin et al., 2019; Brondex et al., 2019). Despite over 60 years of research on basal sliding (e.g., Brondex et al., 2017; Weertman, 1957; Lliboutry, 1958a, b, 1959; Budd et al., 1979; Iken, 1981; Iverson et al., 1998; Tulaczyk et al., 2000; Schoof, 2005; Gagliardini

https://doi.org/10.5194/egusphere-2025-764
Preprint. Discussion started: 17 March 2025

et al., 2007; Tsai et al., 2015; Zoet and Iverson, 2020), the sliding law operating on large scales in Antarctica remains a matter of debate.

For ice that slides over the bed, a no-slip boundary condition is inappropriate. Free slip is also unrealistic because basal drag provides significant resistance to sliding wherever the ice is not floating. Instead, a sliding law that relates basal shear stress to sliding speed is needed. Alternative formulations of this sliding law have been proposed, applying to different subglacial circumstances (e.g., Fig. 1b-f). The frequently used Weertman-type power law (e.g., Weertman, 1957; Arthern et al., 2015; Ritz et al., 2015; Arthern and Williams, 2017; Brondex et al., 2017; Kyrke-Smith et al., 2017; Hank and Tarasov, 2024) considers ice slipping over a rough, hard bed, with ice deforming to pass around large obstacles while bypassing smaller obstacles by pressure melting and regelation (Fig. 1b; Weertman, 1957). In contrast, Lliboutry envisaged discontinuous ice contact with a hard bed, separated by water-filled subglacial cavities (Fig. 1c; Lliboutry, 1958a, b, 1959). Later studies show this cavitation could lead to an upper bound for basal shear stress, even for fast-sliding glaciers (Iken, 1981; Schoof, 2005), and the upper bound was subsequently included in analytically derived sliding laws (Schoof, 2005; Gagliardini et al., 2007).

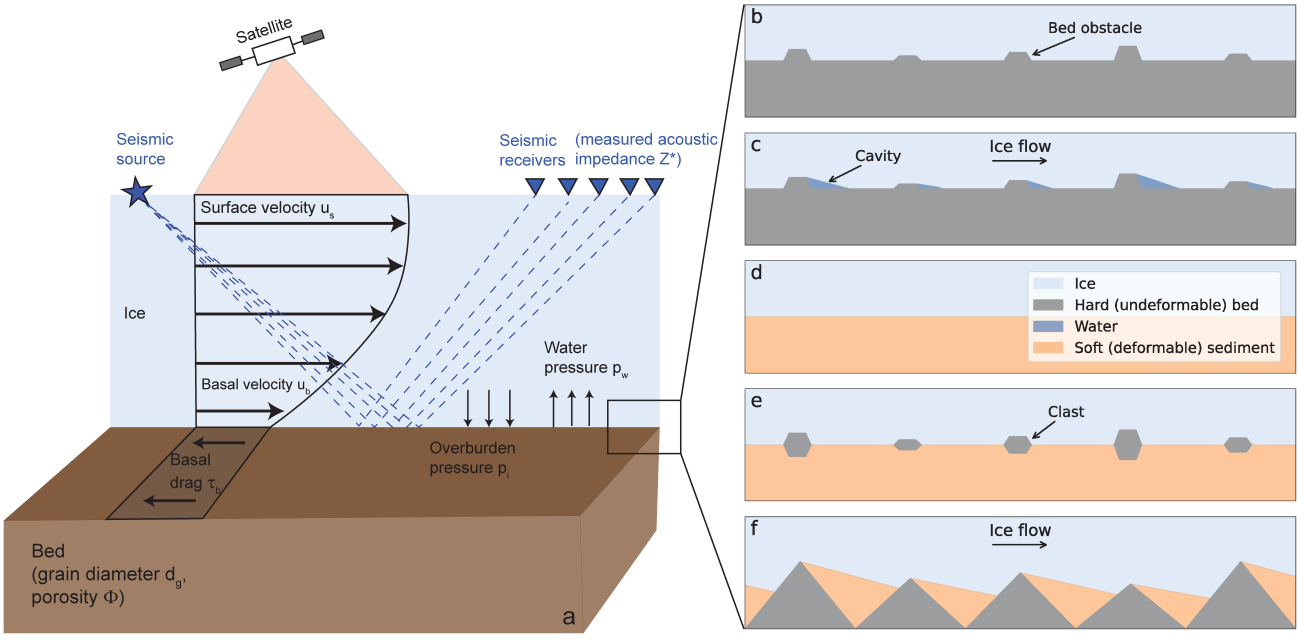

Figure 1. Experimental setup (a) and schematics of the bed considered for different sliding laws (b-f). The schematics are not to scale. Details of the experimental setup are outlined in Fig. 2 and the text.

Another type of basal drag law is based on sliding lubricated by a deforming layer of sediment that yields, either in a rate-dependent (viscoplastic) fashion or according to a rate-independent plastic law (Fig. 1d; e.g., Budd et al., 1979; Iverson et al., 1998; Tulaczyk et al., 2000). One such boundary condition is a Coulomb sliding law, for which the basal shear stress is independent of sliding speed, but varies in proportion to the effective pressure, i.e. the difference between the weight of the overlying ice and the subglacial water pressure. Higher effective pressures lead to greater compression within the granular

https://doi.org/10.5194/egusphere-2025-764
Preprint. Discussion started: 17 March 2025

sediment. In an alternative formulation, a modification of the Weertman-type power law that accounts for a strong dependence of the basal shear stress on effective pressure found in laboratory experiments has been proposed (Budd et al., 1979).

Ice loss projections, particularly of the Amundsen Sea Embayment, are sensitive to the applied sliding law, with sliding law parameters being a key source of uncertainty (e.g., Gillet-Chaulet et al., 2016; Brondex et al., 2017; Joughin et al., 2019; Brondex et al., 2019; Barnes and Gudmundsson, 2022). Previous approaches constraining the basal properties, i.e. the sliding law parameters, generally rely on remote sensing data and inverse methods (e.g., Arthern et al., 2015; Hoffman et al., 2018; Gudmundsson et al., 2019; Ranganathan et al., 2021) or seismic observations (e.g., Smith et al., 2013; Brisbourne et al., 2017) but lack a direct link between observations and the representation of basal sliding in ice sheet models (Kyrke-Smith et al., 2017).

Here, we present a new methodology which enables the quantitative determination of the most appropriate basal sliding law by directly comparing the measured and predicted acoustic impedance, i.e. the product of the compressional wave speed and density of the subglacial material (Fig. 2). The seismic reflection coefficient from the bed is sensitive to the contrast in acoustic impedance between ice and bed. Because the acoustic impedance of ice is known ($3.33 \pm 0.04 \cdot 10^6$ kg m^{-2} s^{-1}; Atre and Bentley, 1993), this allows the acoustic impedance of the bed to be recovered from seismic reflection surveys performed in the field (Fig. 1a). A theory of acoustic propagation in sediment relates the acoustic impedance to the effective pressure, providing a direct link to the basal sliding law: in most laws, low effective pressure, i.e. high basal water pressure, is associated with fast ice sliding over slippery sediment. As basal water pressure has only been measured directly in a few locations via hot-water drilled boreholes (e.g., Engelhardt et al., 1990; Engelhardt and Kamb, 1997; Lüthi et al., 2002; Smith et al., 2021), it has been difficult to map effective pressure. The new approach provides effective pressure over a much wider area.

2 Methods

2.1 Linking seismic observations and basal sliding laws

The six sliding laws examined in this study (Sec. 2.2) are thought to represent sliding over different subglacial beds (Fig. 1b-f). To infer which of these sliding laws is most probable, we first derive the basal shear stress (τ_b) and sliding speed (u_b; Fig. 2 and S1) from inverse methods using the Wavelet-based Adaptive-grid Vertically-integrated Ice-sheet-model (WAVI; Arthern et al., 2015; Bradley et al., 2024, Sec. 2.3). The effective pressure can then be estimated by rearranging the sliding laws. As the Weertman-type power law does not directly depend on effective pressure (N), we instead use two endmember scenarios: a) ice at floatation everywhere ($N = 0$ Pa) and b) ice overburden pressure everywhere ($N = p_\mathrm{i}$; further details in Sec. 2.2.1).

The Viscous Grain-Shearing (VGS) theory (Sec. 2.4; Buckingham, 1997, 2000, 2005, 2007) provides a model of acoustic propagation in granular material. Substituting the estimated effective pressure into this model and using independent estimates for the grain diameter (d_g) and porosity (ϕ) from sediment cores (Engelhardt et al., 1990; Stone and Clarke, 1993; Smith et al., 2011; Kirshner et al., 2012; Smith et al., 2014, 2017; Clark et al., 2024, and Smith, unpublished data), provides an estimate of acoustic impedance for each sliding law. The predicted acoustic impedance is then compared to acoustic impedance measurements collected at five sites on Pine Island Glacier (PIG) in Antarctica (Fig. 4; Brisbourne et al., 2017) by calculating

https://doi.org/10.5194/egusphere-2025-764
Preprint. Discussion started: 17 March 2025

the misfit $\chi^2_{\Theta_i}$ according to

$$\chi^2_{\Theta_i} = \frac{1}{N_\mathrm{d}} \sum_j^{N_\mathrm{d}} \frac{\left(Z_{\Theta_i,j} - Z^*_j\right)^2}{\sigma^2_j}, \tag{1}$$

where $N_\mathrm{d} = 300$ is the number of data points (60 per site, 120 m apart), and $Z_{\Theta_i,j}$ are the acoustic impedance predictions under a given sliding law i and the model parameters Θ_i (grain diameter, porosity, and maximum one additional sliding law parameter). Data points are treated as independent: a sub-sampled data set (every 10th data point) generally yields the same conclusions (Fig. S2). While there is evidence that PIG is largely underlain by deformable sediments (Muto et al., 2016; Brisbourne et al., 2017), the exact values of Θ_i are uncertain. Therefore, the misfit $\chi^2_{\Theta_i}$ is systematically assessed across what is considered to be a reasonable parameter space (Sec. 2.5). The model parameters do not vary spatially. Z^*_j and σ_j are the acoustic impedance observations and their uncertainties. As an example, all metrics involved in predicting the acoustic impedance and calculating the misfit $\chi^2_{\Theta_i}$ (u_b, τ_b, N, Z_{Θ_i}, Z^*, σ) are shown for one set of parameter values ($d_\mathrm{g} = 0.05$ mm, $\phi = 0.43$, transition speed without the dependence on effective pressure $u_{\mathrm{t,noN}} = 708.2\ \mathrm{MPa}^{-1}\ \mathrm{m\ a}^{-1}$) and the Zoet-Iverson sliding law in Fig. S3.

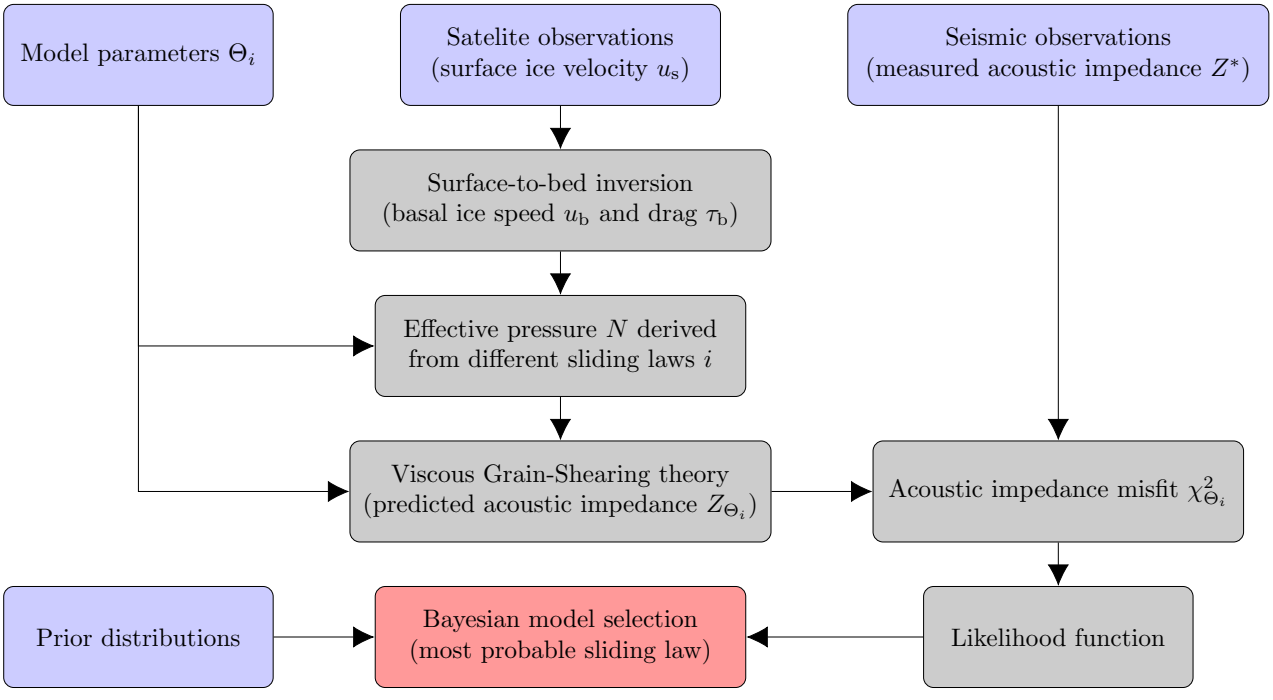

Figure 2. Flowchart of the presented methodology. Refer to the text for further details.

However, inferring the best-candidate sliding law based solely on the minimum misfit is inadequate, as it does not take into account any prior assessment of the probability of the parameter values used. Instead, we use Bayesian model selection

https://doi.org/10.5194/egusphere-2025-764
Preprint. Discussion started: 17 March 2025

(Sec. 2.5) to identify the most probable sliding law based on all misfits within the parameter space (likelihood function in Fig. 2). In this framework, the a priori probability of each model, and of particular parameter values within each model is specified by prior distributions. Using Bayes' rule, these prior probabilities are updated using seismic data, to provide posterior probabilities. Ultimately, this allows us to compute the normalized posterior probability of each sliding law, given the seismic observations collected on PIG (Eq. 18). An advantage of the Bayesian approach is that Occam's razor is automatically applied: overly flexible models with a large range or dimension of parameter space are penalized relative to simpler, less flexible models with fewer parameters or tighter bounds upon parameters.

2.2 Basal sliding laws

The effective pressure required as input for the VGS theory is determined based on the basal sliding laws described here. Usually, these laws are expressed so that basal drag is a function of sliding speed and effective pressure. To compute effective pressures, these relationships must be inverted, either by explicitly rearranging the equations or by numerical root-finding. For all sliding laws and sites, we ensure the effective pressure does not exceed the ice overburden pressure.

2.2.1 Weertman

The Weertman-type power law (Weertman, 1957) assumes that ice slides perfectly over a rigid bed. A thin water film separating the ice and undeformable bed, allows locally for free slip. The basal drag τ_b – resistance to basal motion u_b – is instead induced by form drag as the ice deforms around the bed obstacles (Fig. 1b). This leads to the relationship

$$\tau_\mathrm{b} = C_\mathrm{W} u_\mathrm{b}^m, \tag{2}$$

where C_W and $m = 1/3$ are, respectively, the Weertman friction parameter and exponent (often related to the creep exponent n in Glen's flow law, $m = 1/n$). As Eq. 2 does not directly depend on the effective pressure (N), we calculate the acoustic impedance for two endmember scenarios; a lower bound $N = 0$ Pa for which the ice is assumed to be at floatation everywhere, and an upper bound, $N = p_\mathrm{i}$, for which the effective pressure is assumed equal to the ice overburden pressure (p_i) everywhere. These endmembers correspond, respectively, to situations where basal water pressure fully supports the weight of overlying ice or does not support any weight at all.

2.2.2 Budd

Laboratory experiments examining temperate ice sliding over bed surfaces with a wide range of roughnesses (e.g., Fig. 1b) indicate that τ_b exhibits a strong dependence on N (Budd et al., 1979). Consequently, the Weertman-type power law was modified to account for this dependence.

$$\tau_\mathrm{b} = C_\mathrm{B} u_\mathrm{b}^m N^q, \tag{3}$$

where C_B and $q = 1$ are the Budd friction parameter and exponent, respectively.

https://doi.org/10.5194/egusphere-2025-764
Preprint. Discussion started: 17 March 2025

2.2.3 Coulomb

The Coulomb-type plastic rheology sliding law describes ice sliding over soft, deformable sediments (Fig. 1d; Iverson et al., 1998; Tulaczyk et al., 2000).

$$\tau_\mathrm{b} = \mu N, \tag{4}$$

where $\mu = \tan(\Phi)$ is the Coulomb friction coefficient and Φ the till friction angle.

2.2.4 Tsai-Budd

A simple sliding law describing basal motion as the combination of ice deformation around and across bed obstacles (Weertman) and deformation of the underlying sediment (Coulomb; Fig. 1e or f; Tsai et al., 2015) takes the form

$$\tau_\mathrm{b} = \min[C_\mathrm{W} u_\mathrm{b}^m, \mu N]. \tag{5}$$

Eq. 5 can not be tested in the context discussed here because the Weertman part of the sliding law has no dependence on the effective pressure (using the endmember scenarios for the Weertman part is inconsistent with the underlying assumptions of Eq. 5). To overcome this issue, we replace the Weertman part of Eq. 5 with the Budd sliding law (Eq. 3):

$$\tau_\mathrm{b} = \min[C_\mathrm{B} u_\mathrm{b}^m N^q, \mu N]. \tag{6}$$

When varying C_B, we set $\mu = 0.5$. Similarly, when varying μ, we set $C_\mathrm{B} = 37.01\ \mathrm{m}^{-1/3}\ \mathrm{s}^{1/3}$ (based on minimum misfit when varying C_B).

2.2.5 Schoof

Eq. 2 and 3 neglect Iken's bound induced by water-filled cavities (upper bound of τ_b/N determined by the maximum up-slope angle of the bed in flow direction (β), Fig. 1c; Iken, 1981; Schoof, 2005; Gagliardini et al., 2007). Thus, Schoof (2005) derived a new sliding law incorporating this upper bound. Strictly speaking, the Schoof sliding law only applies to linear ice rheology. Gagliardini et al. (2007) then numerically extended the relationship to non-linear rheologies. Here we use a generalized form of this sliding law (Brondex et al., 2017):

$$\tau_\mathrm{b} = \frac{C_\mathrm{S} u_\mathrm{b}^m}{(1 + (C_\mathrm{S}/(C_\mathrm{max} N))^{1/m} u_\mathrm{b})^m}, \tag{7}$$

where C_S is the Schoof friction parameter and $C_\mathrm{max} = \tan\beta$ represents Iken's bound (Iken, 1981; Schoof, 2005). Initial experiments with $C_\mathrm{S} = 7.624\ \mathrm{MPa\ m}^{-1/3}\ \mathrm{s}^{1/3}$ (as suggested by Brondex et al. (2017)) show a high percentage of incompatible (can not be explained by Eq. 7) $u_\mathrm{b}-\tau_\mathrm{b}$ pairs, inhibiting the determination of a misfit (Fig. S13 and S14; see also Brondex et al., 2019). As varying C_S has only minor effects on the misfit over the examined parameter range (1 to $1 \cdot 10^7\ \mathrm{MPa\ m}^{-1/3}\ \mathrm{s}^{1/3}$; Fig. S13) and to avoid this issue, we set $C_\mathrm{S} = 1 \cdot 10^3\ \mathrm{MPa\ m}^{-1/3}\ \mathrm{s}^{1/3}$ (closest to suggested value while ensuring low percentage of incompatible $u_\mathrm{b}-\tau_\mathrm{b}$ pairs when varying C_max).

https://doi.org/10.5194/egusphere-2025-764
Preprint. Discussion started: 17 March 2025

2.2.6 Zoet-Iverson

Based on experiments in which pressurized ice at its melting temperature is slid over a water-saturated till bed, Zoet and Iverson (2020) derived the following sliding law for glaciers on deformable beds (Fig. 1e):

$$\tau_\mathrm{b} = N\mu\left(\frac{u_\mathrm{b}}{u_\mathrm{b}+u_\mathrm{t}}\right)^{\frac{1}{p}}, \tag{8}$$

where the transition speed

$$u_\mathrm{t} = \frac{\left(\frac{1}{\eta(Ra)^2k_0^3}+\frac{4C_1}{(Ra)^2k_0}\right)(N_F N)}{(2+N_F k)}, \tag{9}$$

$k_0 = \frac{2\pi}{4R}$, and the regelation parameter $C_1 = C_p\frac{K}{L}$. Slightly rearranging Eq. 8 and 9 allows us to numerically determine N

$$\tau_\mathrm{b} = N\mu\left(\frac{u_\mathrm{b}}{u_\mathrm{b}+u_{\mathrm{t,noN}}N}\right)^{\frac{1}{p}}, \tag{10}$$

where

$$u_{\mathrm{t,noN}} = \frac{\left(\frac{1}{\eta(Ra)^2k_0^3}+\frac{4C_1}{(Ra)^2k_0}\right)N_F}{(2+N_F k)} \tag{11}$$

is the transition speed without the dependence on N. All other parameters are listed in Table. 1.

Variable	Description	Value	Unit
p	slip exponent	5	-
η	effective ice viscosity	$3.2\cdot10^{12}$	Pa s
R	clast radius	0.0153	m
a	fraction of clast radius that protrudes from bed surface	0.25	-
C_p	depression of the melting temperature of ice with pressure	$7.4\cdot10^{-8}$	K Pa^{-1}
K	mean thermal conductivity of ice and rock	2.55	W m^{-1} K^{-1}
L	volumetric latent heat of ice	$3\cdot10^{8}$	J m^{-3}
N_f	till bearing capacity factor	33	-
k	till strength reduction resulting from the ice pressure shadow in the lee of clasts	0.1	-

Table 1. Parameters used in Eqs. 10 and 11 (supplementary material of Zoet and Iverson (2020) and references therein).

2.3 Surface-to-bed inversion

Basal shear stress and basal sliding speed are derived using the ice sheet model WAVI, which is vertically integrated but retains an implicit velocity-depth profile (Arthern et al., 2015; Bradley et al., 2024). Data assimilation methods are used to initialise

https://doi.org/10.5194/egusphere-2025-764
Preprint. Discussion started: 17 March 2025

the model into a present-day state (approximately 2015): spatially varying two-dimensional fields of ice stiffness and basal drag are calculated by matching modelled surface velocities with observations of surface velocities (Mouginot et al., 2022), accumulation rates (Arthern et al., 2006), and thinning rates (Smith et al., 2020). Internal ice temperatures are provided from a thermal solve of the BISICLES ice sheet model (Cornford et al., 2013). Full details of the inverse method are detailed in Arthern et al. (2015), and the resulting basal sliding speed and basal shear stress are shown in Fig. S1. In this inversion, the basal drag is identified using the Weertman sliding law. However, the sliding relationship that links basal drag and basal speed can be re-parameterised in terms of any of the selected sliding laws that we test here, as long as neither the basal speed nor the basal drag are altered in this process.

2.4 Viscous Grain-Shearing theory

The Viscous Grain-Shearing (VGS) theory (Buckingham, 1997, 2000, 2005, 2007) is used to relate seismic observations to effective pressure (Fig. 2). According to the VGS, the elastic deformation under effective pressure that generates frictional resistance also stiffens the sediment and increases the speed of propagation of sound waves. Changes in the speed of sound alter the acoustic impedance ($Z = \rho_s c_p$), the product of the compressional wave speed in the sediment (c_p) and density (ρ_s). In turn, the acoustic impedance controls the reflection coefficient of seismic energy from the base of the ice sheet. The acoustic propagation model predicts the compressional wave speed ($c_p = \psi[N, d_g, \phi, f_s]$) as a function of effective pressure (N), grain diameter (d_g), porosity (ϕ), and seismic frequency (f_s). The link between the compressional wave speed and effective pressure predicted by the acoustic model provides an avenue to test whether a given sliding law applies at any location. All other parameters of the acoustic propagation model have been calibrated using acoustic observations of the ocean floor.

The governing equation for the compressional wave speed is

$$c_p = \frac{c_0}{\mathrm{Re}\left[1 + \zeta\,(i\omega T)^q\, g\,(\omega\tau_p)\right]^{-1/2}}, \tag{12}$$

where $c_0 = \sqrt{\frac{\kappa_0}{\rho_0}}$ is the sound speed in the absence of grain-to-grain interactions, $\kappa_0 = \left(\frac{\phi}{\kappa_p} + \frac{1-\phi}{\kappa_g}\right)^{-1}$ the bulk modulus of the medium, and $\rho_0 = \phi\rho_p + (1-\phi)\rho_g$ the bulk density of the medium. The dimensionless grain-shearing coefficient is

$$\zeta = \frac{\gamma_p + (4/3)\,\gamma_s}{\rho_0 c_0^2}, \tag{13}$$

where $\gamma_p = \gamma_{p0}\left[\frac{N d_g}{N_0 d_{g0}}\right]^{1/3}$ and $\gamma_s = \gamma_{s0}\left[\frac{N d_g}{N_0 d_{g0}}\right]^{2/3}$ are the compressional and shear rigidity coefficients, respectively. $N_0 = (1-\phi_0)(\rho_g - \rho_p) g z_0$ is the reference effective pressure. The function

$$g\,(\omega\tau_p) = \left(1 + \frac{1}{i\omega\tau_p}\right)^{-1+q} \tag{14}$$

accounts for the effect of the viscosity of the molecularly thin layer of pore fluid between contiguous grains (ν). Molecularly thin films become progressively more viscous as they are squeezed, and, therefore, ν differs significantly from the viscosity of the bulk fluid (Israelachvili, 1986; Luengo et al., 1996; Granick, 1999). The compressional viscoelastic time constant τ_p is

https://doi.org/10.5194/egusphere-2025-764
Preprint. Discussion started: 17 March 2025

defined as $\tau_\mathrm{p} = \nu/E$, where E is a spring constant (Buckingham, 2005). The values of τ_p used in the VGS theory are visual fits to the *SAX99* experiments (Buckingham, 2007). However, the measurements were taken in 18 to 19 m deep water (Richardson et al., 2001). Therefore, the exerted overburden pressure is ~ 2 orders of magnitude smaller (less squeezed) than under PIG (ice thickness of 1500 to 2500 m in tributaries, e.g., Fretwell et al., 2013). While it is apparent that the viscosity of molecularly thin layers increases with the applied pressure (or loading) p_L, the exact relationship between p_L, the thickness of the thin film, and the viscosity ν is not straightforward (e.g., Israelachvili, 1986; Luengo et al., 1996; Yamada, 2003). Assuming $\nu \propto p_\mathrm{L}$, we set $\tau_\mathrm{p} = 0.012$ s (2 orders of magnitude larger than the value in Buckingham, 2007)).

$\omega = 2\pi f$ is the angular frequency, $i = \sqrt{-1}$, and Re returns the real part of a complex number. All other parameters are listed in Table 2.

Variable	Description	Value	Unit
T	arbitrary time introduced to avoid awkward dimensions	1	s
q	strain hardening index	0.0851	-
κ_p	bulk modulus of pores	$2.374 \cdot 10^9$	Pa
κ_g	bulk modulus of grains	$3.6 \cdot 10^{10}$	Pa
ρ_p	density of pore fluid	1005	kg m^{-3}
ρ_g	density of grains	2730	kg m^{-3}
$\gamma_{\mathrm{p}0}$	reference compressional coefficient	$3.888 \cdot 10^8$	Pa
$\gamma_{\mathrm{s}0}$	reference shear coefficient	$4.588 \cdot 10^7$	Pa
$d_{\mathrm{g}0}$	reference grain diameter	$1 \cdot 10^{-1}$	m
ϕ_0	reference porosity	0.377	-
g	acceleration due to gravity	9.81	m s^{-2}
z_0	reference depth in sediment	0.3	m
f_s	seismic frequency	100	Hz
τ_p	compressional viscoelastic time constant	0.012	s

Table 2. Parameters used in the VGS theory. The values for f_s and τ_p are based on seismic frequencies in a glaciological context and a scaling analysis of the value used in Buckingham (2007), respectively. All other values are adopted from Buckingham (2005).

2.5 Bayesian model selection

We compare the different sliding laws using Bayes Rule:

$$P(M_i|D) = \frac{P(D|M_i)\, P(M_i)}{P(D)}, \tag{15}$$

where M_i represents the model for sliding law i (together with VGS theory) and D represents the data (acoustic impedance observations). Since the number of parameters differs between models, we marginalize over the model parameters Θ_i to retrieve

https://doi.org/10.5194/egusphere-2025-764
Preprint. Discussion started: 17 March 2025

$P(D|M_i)$:

$$P(D|M_i) = \int_{\Theta_i} P(D|\Theta_i, M_i)\ P(\Theta_i|M_i)\, d\Theta_i. \tag{16}$$

Assuming the error of the data follows a Gaussian distribution, the likelihood of the data given the model and parameters is calculated according to

$$P(D|\Theta_i, M_i) = \exp\left(-0.5\chi^2_{\Theta_i}\right). \tag{17}$$

Therefore, the posterior probability of each model M_i is

$$P(M_i|D) = \frac{\int_{\Theta_i} \exp\left(-0.5\chi^2_{\Theta_i}\right)\ P(\Theta_i|M_i)\, d\Theta_i\ P(M_i)}{\sum_{j=1}^{n} \int_{\Theta_j} \exp\left(-0.5\chi^2_{\Theta_j}\right)\ P(\Theta_j|M_j)\, d\Theta_j\ P(M_j)}, \tag{18}$$

where we use a prior $P(M_i) = 1/n$ that considers each sliding law equally probable, with n being the number of sliding laws considered.

Finally, the prior distributions for all model parameters $P(\Theta_i|M_i)$ need to be defined. The prior distributions for all individual parameters are shown in Fig. 3. The combination of multiple individual priors creates a model's parameter space Θ_i and determines the model prior $P(\Theta_i|M_i)$. Since the parameter space differs between the models (number of individual parameters (dimensions) as well as number of tested parameter values), we ensure $\int_{\Theta_i} P(\Theta_i|M_i)\, d\Theta_i = 1$ for all models. This normalization penalizes models with a larger parameter space.

Various literature estimates inform the examined parameter ranges and corresponding prior distributions. The porosity prior (Fig. 3a) is derived from borehole data and seismic experiments from Ice Stream B and C, West Antarctica (Blankenship et al., 1987; Engelhardt et al., 1990; Atre and Bentley, 1993), borehole data from Trapridge Glacier, Yukon Territory, Canada (Stone and Clarke, 1993), marine sediment cores from the Amundsen Sea Embayment (Smith et al., 2011, 2014, 2017), sediment recovered from beneath Rutford Ice Stream, West Antarctica (Smith, unpublished data), as well as the porosity of sands and glass beads used to validate the VGS (Buckingham, 2014; Lee et al., 2016, and references therein). As the latter do not directly relate to a glacial context, we assign these higher porosities a lower probability. The grain diameter prior (Fig. 3b) is based on sediment cores collected in the Amundsen Sea Embayment, particularly Pine Island Bay (Kirshner et al., 2012; Smith et al., 2011, 2014, 2017; Clark et al., 2024) and the Rutford ice stream (Smith, unpublished data). We differentiate between Clay ($< 1/256$ mm), Silt ($\geq 1/256$ mm and $\leq 1/16$ mm), and Sand ($> 1/16$ mm). A log-uniform prior was chosen for $u_{\mathrm{t,noN}}$ (Fig. 3c) as it is a positive scale that depends on several uncertain parameters and no constraints beyond the initial publication are available (Zoet and Iverson, 2020). The $C_{\max}$ prior (Fig. 3d) is based on bed topography beneath PIG retrieved from Bedmap2 data (Fig. S4 and S5; Fretwell et al., 2013) as well as autonomous underwater vehicle (AUV) data collected downstream of Thwaites Glacier (Graham et al., 2022) and under the Thwaites Eastern Ice Shelf (Wåhlin, unpublished data; Fig. S6 and S7). μ is a frequently used parameter and its prior (Fig. 3e) aims to capture the overall distribution within the glaciological community (e.g., Savage et al., 2000; Tulaczyk et al., 2000; Cuffey and Paterson., 2010; Iverson, 2010; Tsai et al., 2015; Brondex et al., 2017). As C_{B} and C_{S} are positive scaling coefficients that may vary over several orders of magnitude,

https://doi.org/10.5194/egusphere-2025-764
Preprint. Discussion started: 17 March 2025

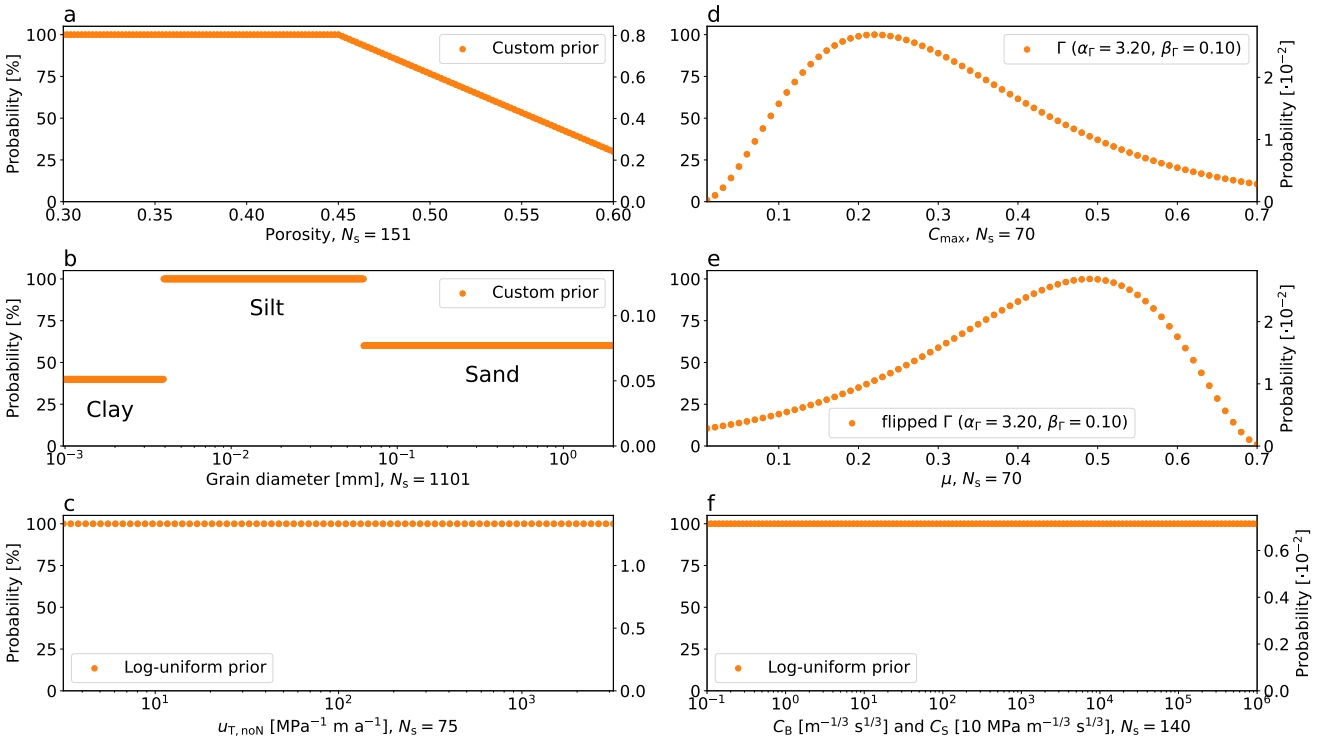

Figure 3. Prior distributions for all model parameters Θ. N_s is the sampling size. The left and right axes show the scaled probability (0 to 100 %) and actual probability used (depends on N_s), respectively.

even within the same glacial catchment (Budd et al., 1984; Larour et al., 2012; Favier et al., 2014; Arthern et al., 2015; Brondex et al., 2017; Gladstone et al., 2017), a log-uniform prior was chosen for these parameters (Fig. 3f).

3 Results and Discussion

3.1 Minimum acoustic impedance misfit comparable for all sliding laws examined

Based on a previous study examining the same acoustic impedance data (Kyrke-Smith et al., 2017) and due to the smoothing effect of the inversion (1 km horizontal grid resolution), we do not expect to capture acoustic impedance variations for each individual data point but rather the general trend across the five data sites. Given this context, all sliding laws reasonably match the acoustic impedance observations when using the parameter values yielding the minimum misfit across all data sites (Fig. 4). However, for some sliding laws, the minimum misfit parameter values are at the limits of the likely range (e.g., extremely small grain diameter ($d_g = 0.003$ mm) for the Budd sliding law). As an example, Fig. 5 shows how the misfit varies with the three model parameters d_g, ϕ, and $u_{t,noN}$ when using a Zoet-Iverson sliding law. The same plots for all other sliding laws are shown in Fig. S8 to S19. While the minimum misfit might correspond to a rather unlikely parameter value, a narrow band of

https://doi.org/10.5194/egusphere-2025-764
Preprint. Discussion started: 17 March 2025

similarly small misfits spans a more reasonable parameter range, indicating some indistinctness in the selected minimum misfit parameter values. This is a key characteristic of the misfit distribution in all of our experiments.

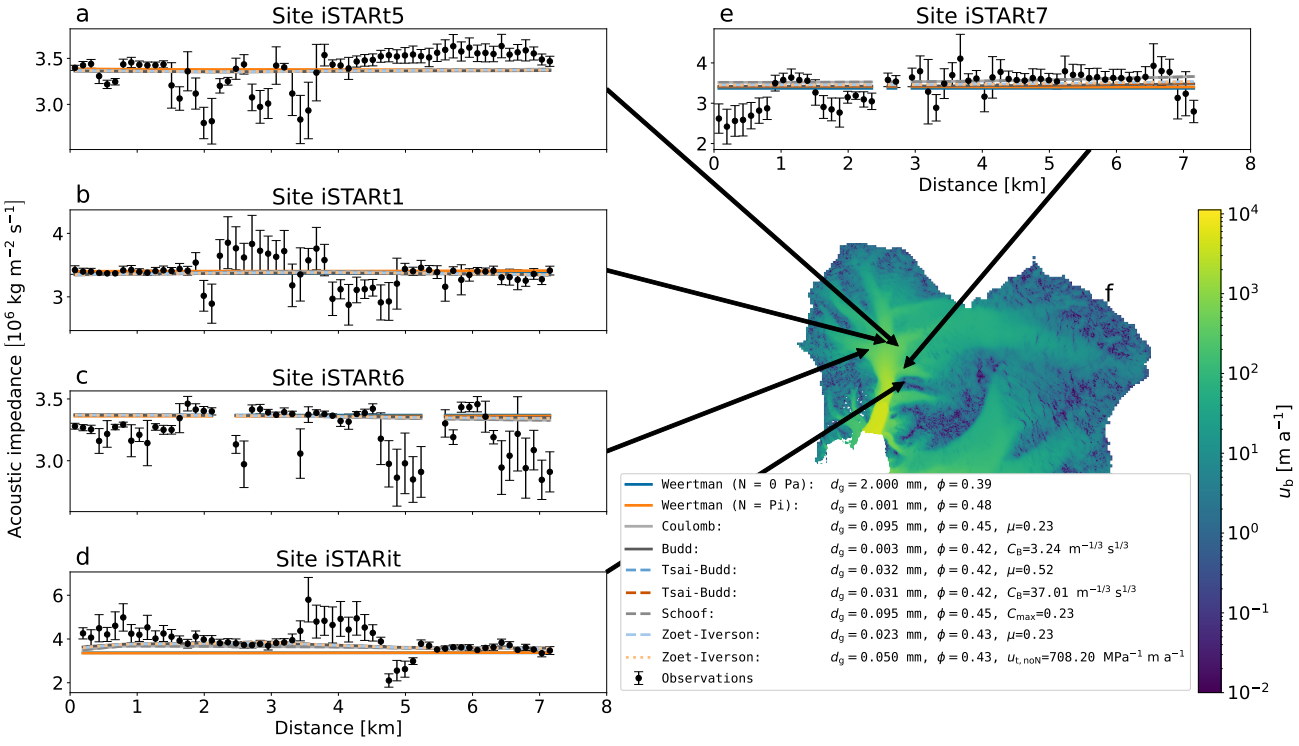

Figure 4. (a-e) Acoustic impedance observations (Brisbourne et al., 2017) compared with the model predictions based on different sliding laws when using the minimum misfit model parameters shown in the legend. The observational uncertainties are shown as error bars. The model parameters are grain diameter (d_g), porosity (ϕ), Coulomb friction coefficient (μ), Budd friction parameter (C_B), Iken's bound (C_{max}), and transition speed without the dependence on effective pressure N ($u_{t,noN}$; see Sec. 2.2 for details). (f) Basal sliding speed in the Amundsen Sea Embayment (from inversion; Sec. 2.3). The arrows mark the location of the data sites. Except for site iSTARit, all data were collected on fast-flowing tributaries of PIG (Brisbourne et al., 2017).

3.2 Ice dynamics of Pine Island Glacier governed by Coulomb-type sliding

To consider any prior assessment of the probability of the parameter values used and the misfit distribution across the entire parameter range, we infer the best-candidate sliding law based on Bayesian model selection. The Zoet-Iverson sliding law when varying $u_{t,noN}$ has the highest posterior probability of all sliding laws tested (increase of 22 %; Fig. 6). The Coulomb, Tsai-Budd, Schoof, and Zoet-Iverson sliding laws all show an increase in probability relative to the prior. All of these laws incorporate a Coulomb friction term of the form μN or $C_{max}N$, suggesting this is a desirable property of a sliding law. In comparison, the Budd sliding law, without the μN modification of the Tsai-Budd law, performs worse (5.6 % decrease). The Weertman-type endmember scenario that assumes $N = p_i$ everywhere performs worst of all, leading to the smallest posterior

https://doi.org/10.5194/egusphere-2025-764
Preprint. Discussion started: 17 March 2025

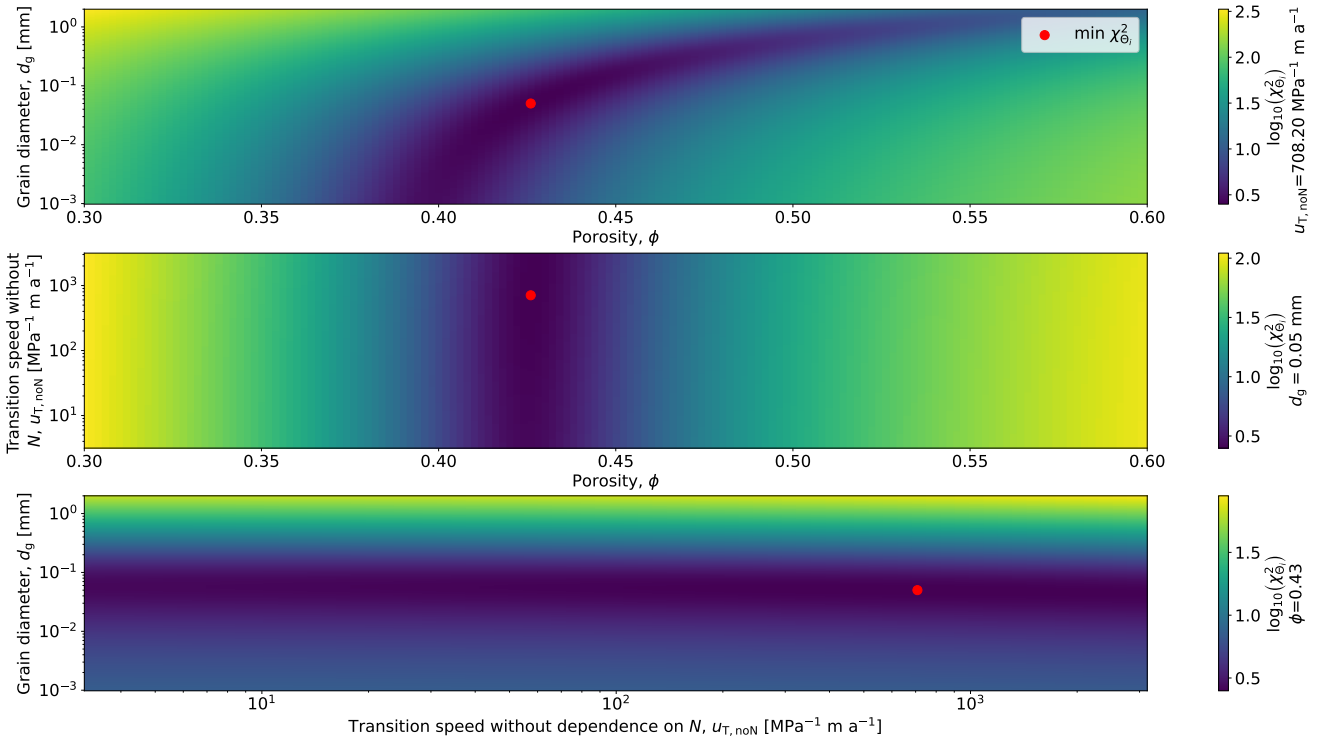

Figure 5. Variations of the misfit $\chi^2_{\Theta_i}$ with the three model parameters grain diameter (d_g), porosity (ϕ), and transition speed without the dependence on N $(u_{t,noN})$ under a Zoet-Iverson sliding law (Coulomb friction coefficient μ fixed at 0.5; see Sec. 2.2.6 for details). For the parameter not shown, the value yielding the minimum misfit is used and denoted next to the colorbar of the corresponding panel. The red dots mark the minimum misfit.

probability (84.2 % decrease). The endmember scenario with $N = 0$ Pa everywhere yields the highest posterior probability of all sliding laws that do not incorporate a Coulomb friction term (1.1 % decrease; see Fig. S20 for the Weertman-type power law when using different fractions of the overburden pressure as effective pressure).

The relatively high posterior probabilities of sliding laws incorporating a Coulomb friction term and the $N = 0$ Pa endmember scenario are consistent with the widespread occurrence of deformable sediment under the fast-flowing tributaries of PIG (Brisbourne et al., 2017). Furthermore, the high probabilities of these sliding laws align with previous studies identifying (quasi-)plastic deformation of the underlying sediment as the primary mode of sliding for PIG (Gillet-Chaulet et al., 2016; Joughin et al., 2019). While the sensitivity of grounding-line retreat patterns and mass loss projections to the choice of sliding law is high (Brondex et al., 2019), determining the exact implications of using a (quasi-)plastic sliding law on glacier behaviour through prognostic simulations for all sliding laws and parameter values is out of the scope of this study. In general, sliding laws representing a (quasi-)plastic rheology lead to higher sea level rise contributions (Ritz et al., 2015; Gillet-Chaulet et al., 2016; Brondex et al., 2019).

https://doi.org/10.5194/egusphere-2025-764
Preprint. Discussion started: 17 March 2025

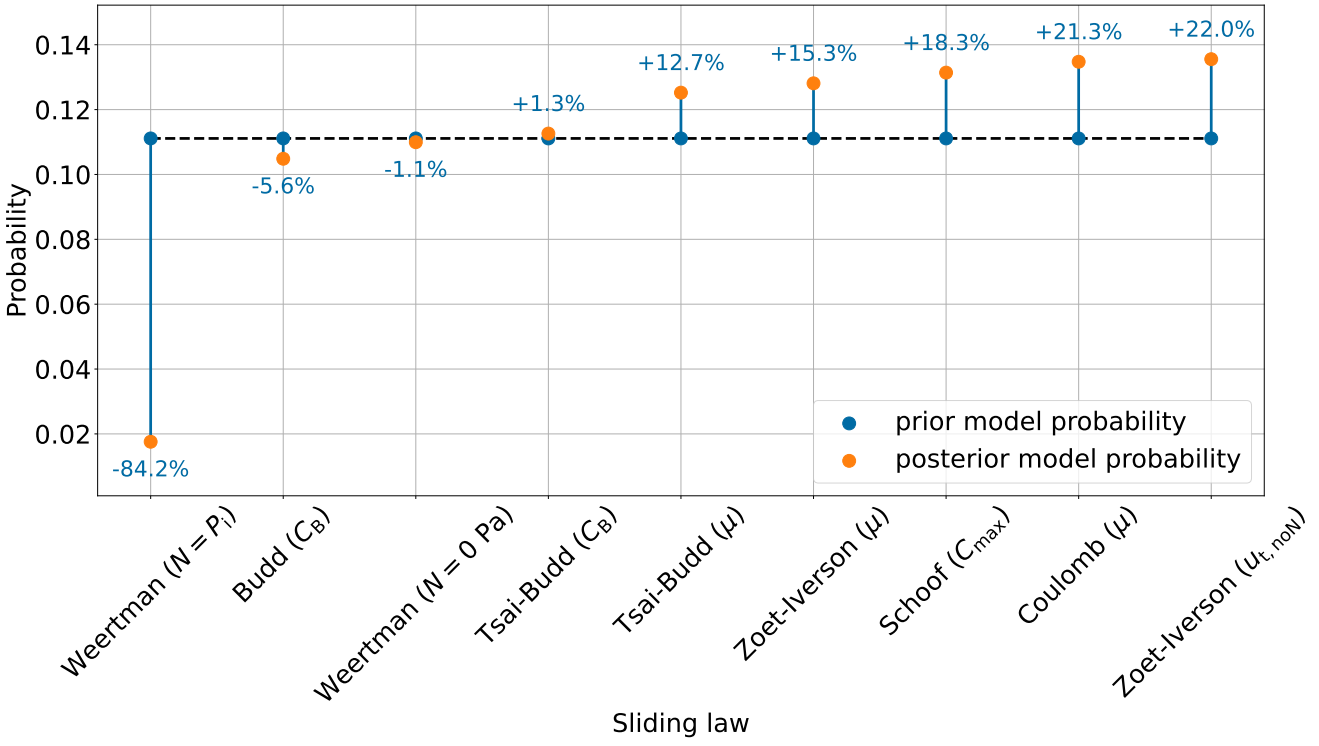

Figure 6. Normalized probabilities of all sliding laws examined in this study given the acoustic impedance observations collected on PIG. The prior model probability is $P(M_i) = 1/n$, with n being the number of models examined (blue circles; dashed horizontal line visualizes equal prior probability). To obtain the posterior model probability, we marginalized over all corresponding model parameters Θ_i, encompassing the acoustic propagation model parameters (d_g and ϕ) and varied sliding law parameters (denoted in brackets). No sliding law parameter was varied for the two Weertman-type endmember scenarios as they use a fixed effective pressure ($N = p_i$ and $N = 0$ Pa). The prior distributions for all parameters are shown in Fig. 3. The blue vertical lines and numbers indicate the change in probability.

3.3 Effect of prior distributions on most probable model parameters

As for the minimum misfit model parameters, the predicted acoustic impedance under the model parameters with the highest posterior probability generally agrees with the observations within uncertainties for all sliding laws tested (Fig. S21). In the remainder of this paper, we refer to the model parameters with the highest posterior probability as the maximum a posteriori (MAP) parameters. When examining the MAP parameters in more detail, the effect of the chosen prior distributions is evident. Although covering the full range within this size classification, the MAP grain diameter for all sliding laws is Silt-sized (highest prior probability; Fig. 3). The MAP porosities (0.39 to 0.44) are at the upper end of the high-prior probability range ($\phi = [0.3, 0.45]$) for all sliding laws except the Weertman-type endmember scenario $N = p_i$ ($\phi = 0.55$; Fig. S21), indicating comparatively porous sediments beneath PIG. Similarly, the MAP values of the unique sliding law parameters without a log-uniform prior distribution (μ and $C_{\max}$) are in the vicinity of the highest prior probability.

https://doi.org/10.5194/egusphere-2025-764
Preprint. Discussion started: 17 March 2025

Even if we use log-uniform prior distributions for scaling coefficients and uniform priors for other parameters, the sliding laws incorporating a Coulomb friction term still yield the highest probabilities (Fig. S22). This demonstrates the robustness of our key result against variations in prior distributions.

3.4 Low effective pressure across most of Amundsen Sea Embayment

Excluding the two Weertman-type endmember scenarios (fixed N), the predicted effective pressure for the MAP model parameters is generally below 0.1 MPa (1 bar) for the 4 sites within fast-flowing tributaries (Fig. S23). The relatively high probability of the $N = 0$ Pa Weertman-type endmember scenario (Fig. S20) further supports a low effective pressure. This is in agreement with previous effective pressure estimates derived from, e.g., shear wave velocities (Blankenship et al., 1987), borehole water level measurements (Engelhardt et al., 1990; Engelhardt and Kamb, 1997; Lüthi et al., 2002; Smith et al., 2021), and the widespread presence of active subglacial lakes (Gray et al., 2005; Fricker et al., 2007; Smith et al., 2009).

Site iSTARit, located between two tributaries, has higher effective pressures (0.1 to 1 MPa), with the effective pressure derived from the Zoet-Iverson sliding law being ~ 0.5 MPa. We hypothesize that the higher effective pressure and resulting increased basal drag at this site hinder basal sliding.

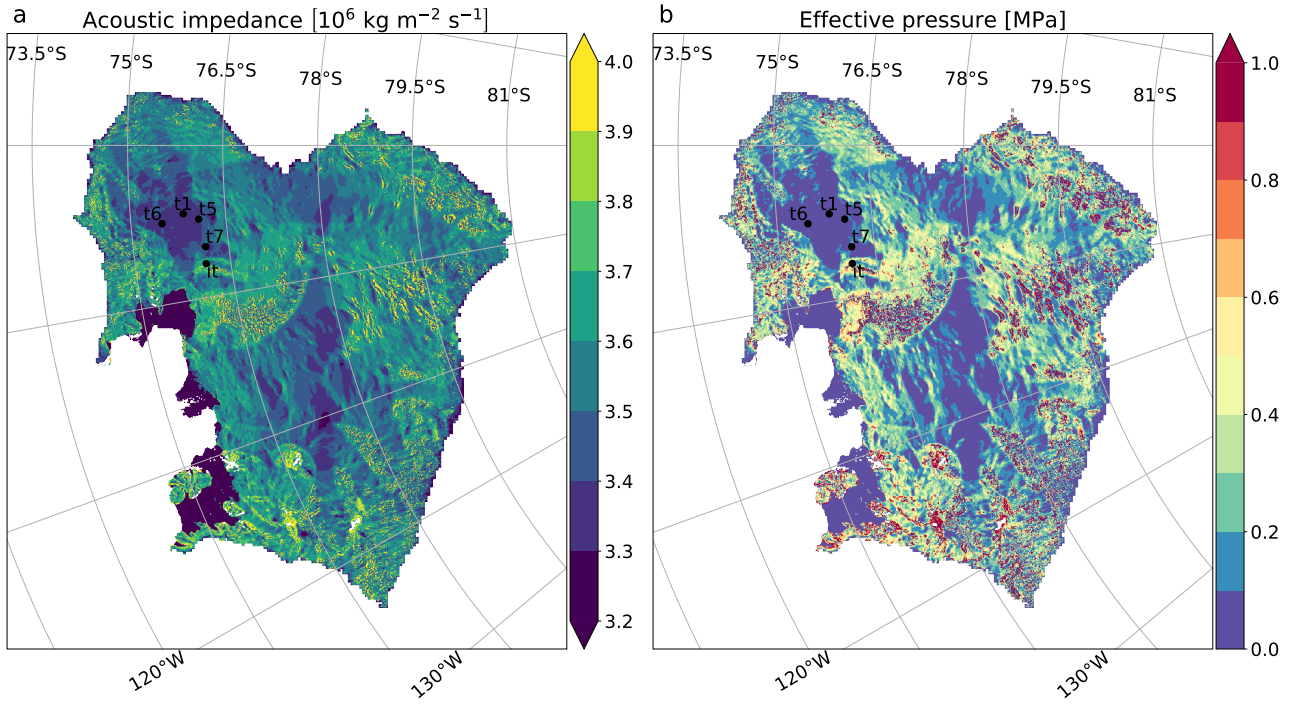

Figure 7. Predicted acoustic impedance (a) and effective pressure (b) in the Amundsen Sea Embayment when using a Zoet-Iverson sliding law with the MAP (highest posterior probability) model parameters ($d_{\mathrm{g}} = 0.05$ mm, $\phi = 0.43$, and $u_{\mathrm{t,noN}} = 708.2$ MPa^{-1} m a^{-1}). The black dots mark the locations of the seismic observation sites.

https://doi.org/10.5194/egusphere-2025-764
Preprint. Discussion started: 17 March 2025

Retrieving the effective pressure for the Zoet-Iverson ($u_{\mathrm{t,noN}}$) sliding law with the MAP parameters across the whole Amundsen Sea Embayment indicates the effective pressure is generally below 0.5 MPa (Fig. 7b). Being closely related to the basal drag, this map represents the slipperiness of the bed, with areas of low effective pressure being susceptible to fast retreat. However, the effective pressure map is based on a spatially uniform $u_{\mathrm{t,noN}}$ obtained from five sites in PIG and does not capture (local) dynamic subglacial systems as, e.g., represented by a subglacial hydrology model. Furthermore, using only the Zoet-Iverson ($u_{\mathrm{t,noN}}$) sliding law with the MAP parameters neglects the probabilities of other sliding laws and parameter values. Following the Bayesian framework to account for these probabilities and determine the most probable effective pressure map by weighting the individual maps for all sliding laws and parameter values, as well as using spatially variable model parameters is out of the scope of this study. Therefore, the provided effective pressure map should be used with caution.

4 Conclusions

In this study, we present a new approach that directly relates measured and predicted acoustic impedance data to infer an ice sheet sliding law and, subsequently, effective pressure. While the current conclusions are primarily based on seismic data over soft sediments, the presented methodology can be readily applied to any acoustic impedance data collected in a glacial environment. For the seismic data collected on fast-flowing tributaries of Pine Island Glacier, the acoustic propagation model predicts the observed acoustic impedance within uncertainties. Inferred effective pressures are generally below 0.5 MPa across most of the Amundsen Sea Embayment and below 0.1 MPa within fast-flowing tributaries of Pine Island Glacier. Bayesian model selection identifies Coulomb behaviour as the most probable mode of sliding, potentially increasing sea level rise contributions from the Amundsen Sea Embayment. To minimize uncertainties in sea level rise projections, the sliding law used in large-scale ice sheet models should, therefore, approach Coulomb behaviour in fast-flowing regions.

Code availability. The main code has been attached to the submission of this manuscript. After acceptance for publication, the code will be made available in a public archive.

Data availability. Data is available upon request from the corresponding author. After acceptance for publication, the data will be made available in a public archive.

https://doi.org/10.5194/egusphere-2025-764
Preprint. Discussion started: 17 March 2025

310

Author contributions. KH, RJA, and CRW conceptualized the ideas behind this study. AMB, JAS, and AW prepared, respectively, the seismic data, sediment core data, and AUV data for use in this study. KH prepared the experimental design, ran the model, and analyzed the results with input from all authors. All authors contributed to the interpretation of the results and writing of the paper.

Competing interests. The authors have no competing interests.

315

Acknowledgements. The authors thank the members of the International Thwaites Glacier Collaboration (ITGC), particularly the ITGC Geophysical Habitat of Subglacial Thwaites (GHOST) team for fruitful discussion. We also thank Ronan S. Agnew and Kelly A. Hogan for their support in the interpretation of acoustic impedance and autonomous underwater vehicle (AUV) data, respectively.

This work was funded by the GHOST project, a component of the International Thwaites Glacier Collaboration (ITGC). Support from
320 National Science Foundation (NSF: Grant PLR 1738934) and Natural Environment Research Council (NERC: Grant NE/S006672/1), with logistics provided by NSF-U.S. Antarctic Program and NERC-British Antarctic Survey. ITGC Contribution No. ITGC-142. Additional support was provided by the ITGC MELT project (NSF Grant 1739003 and NERC Grant NE/S006656/1) and Natural Environment Research Council (NERC: Grant NE/G014159/1 and NE/R016038/1). The Ran AUV was financed by Knut and Alice Wallenberg Foundation.

https://doi.org/10.5194/egusphere-2025-764
Preprint. Discussion started: 17 March 2025

References

Arthern, R. J. and Williams, C. R.: The sensitivity of West Antarctica to the submarine melting feedback, Geophysical Research Letters, 44, 2352–2359, https://doi.org/10.1002/2017GL072514, 2017.

Arthern, R. J., P. Winebrenner, D., and Vaughan, D.: Antarctic Snow Accumulation Mapped Using Polarization of 4.3-cm Wavelength Microwave Emission, Journal of Geophysical Research, 111, D06 108, https://doi.org/10.1029/2004JD005667, 2006.

Arthern, R. J., Hindmarsh, R. C., and Williams, C. R.: Flow speed within the Antarctic ice sheet and its controls inferred from satellite observations, Journal of Geophysical Research: Earth Surface, 120, 1171–1188, https://doi.org/10.1002/2014JF003239, 2015.

Atre, S. R. and Bentley, C. R.: Laterally varying basal conditions beneath ice Streams B and C, West Antarctica, Journal of Glaciology, 39, 507–514, https://doi.org/10.3189/s0022143000016403, 1993.

Barnes, J. M. and Gudmundsson, G. H.: The predictive power of ice sheet models and the regional sensitivity of ice loss to basal sliding parameterisations: a case study of Pine Island and Thwaites glaciers, West Antarctica, The Cryosphere, 16, 4291–4304, https://doi.org/10.5194/tc-16-4291-2022, 2022.

Blankenship, D. D., Bentley, C. R., Rooney, S. T., and Alley, R. B.: Till beneath ice stream B. 1. Properties derived from seismic travel times, Journal of Geophysical Research, 92, 8903–8911, https://doi.org/10.1029/JB092iB09p08903, 1987.

Bradley, A. T., Arthern, R. J., Bett, D. T., Williams, C. R., and Byrne, J.: WAVI.jl: Ice Sheet Modelling in Julia, Journal of Open Source Software, 9, 5584, https://doi.org/10.21105/joss.05584, 2024.

Brisbourne, A. M., Smith, A. M., Vaughan, D. G., King, E. C., Davies, D., Bingham, R. G., Smith, E. C., Nias, I. J., and Rosier, S. H.: Bed conditions of Pine Island Glacier, West Antarctica, Journal of Geophysical Research: Earth Surface, 122, 419–433, https://doi.org/10.1002/2016JF004033, 2017.

Brondex, J., Gagliardini, O., Gillet-Chaulet, F., and Durand, G.: Sensitivity of grounding line dynamics to the choice of the friction law, Journal of Glaciology, 63, 854–866, https://doi.org/10.1017/jog.2017.51, 2017.

Brondex, J., Gillet-Chaulet, F., and Gagliardini, O.: Sensitivity of centennial mass loss projections of the Amundsen basin to the friction law, The Cryosphere, 13, 177–195, https://doi.org/10.5194/tc-13-177-2019, 2019.

Buckingham, M. J.: Theory of acoustic attenuation, dispersion, and pulse propagation in unconsolidated granular materials including marine sediments, The Journal of the Acoustical Society of America, 1997.

Buckingham, M. J.: Wave propagation, stress relaxation, and grain-to-grain shearing in saturated, unconsolidated marine sediments, 2000.

Buckingham, M. J.: Compressional and shear wave properties of marine sediments: Comparisons between theory and data, The Journal of the Acoustical Society of America, 117, 137–152, https://doi.org/10.1121/1.1810231, 2005.

Buckingham, M. J.: On pore-fluid viscosity and the wave properties of saturated granular materials including marine sediments, The Journal of the Acoustical Society of America, 122, 1486–1501, https://doi.org/10.1121/1.2759167, 2007.

Buckingham, M. J.: Analysis of shear-wave attenuation in unconsolidated sands and glass beads, The Journal of the Acoustical Society of America, 136, 2478–2488, https://doi.org/10.1121/1.4896468, 2014.

Budd, W. F., Keage, P. L., and Blundy, N. A.: Empirical Studies of Ice Sliding, Journal of Glaciology, 23, 157–170, https://doi.org/10.3189/s0022143000029804, 1979.

Budd, W. F., Jenssen, D., and Smith, I. N.: A Three-Dimensional Time-Dependent Model of the West Antarctic Ice Sheet, Annals of Glaciology, 5, 29–36, https://doi.org/10.3189/1984aog5-1-29-36, 1984.

https://doi.org/10.5194/egusphere-2025-764
Preprint. Discussion started: 17 March 2025

Clark, R. W., Wellner, J. S., Hillenbrand, C. D., Totten, R. L., Smith, J. A., Miller, L. E., Larter, R. D., Hogan, K. A., Graham, A. G., Nitsche, F. O., Lehrmann, A. A., Lepp, A. P., Kirkham, J. D., Fitzgerald, V. T., Garcia-Barrera, G., Ehrmann, W., and Wacker, L.: Synchronous retreat of Thwaites and Pine Island glaciers in response to external forcings in the presatellite era, Proceedings of the National Academy of Sciences of the United States of America, 121, https://doi.org/10.1073/pnas.2211711120, 2024.

Cornford, S. L., Martin, D. F., Graves, D. T., Ranken, D. F., Le Brocq, A. M., Gladstone, R. M., Payne, A. J., Ng, E. G., and Lipscomb, W. H.: Adaptive mesh, finite volume modeling of marine ice sheets, Journal of Computational Physics, 232, 529–549, https://doi.org/https://doi.org/10.1016/j.jcp.2012.08.037, 2013.

Cuffey, K. and Paterson., W.: The Physics of Glaciers, Butterworth-Heinemann/Elsevier, Burlington, MA, 4th edn., 2010.

Engelhardt, H. and Kamb, B.: Basal hydraulic system of a west Antartic ice stream: constraints from borehole observations, Journal of Glaciology, 43, 207–230, https://doi.org/10.3189/s0022143000003166, 1997.

Engelhardt, H., Humphrey, N., Kamb, B., and Fahnestock, M.: Physical Conditions at the Base of a Fast Moving Antarctic Ice Stream, Science, 248, 57–59, https://doi.org/10.1126/science.248.4951.57, 1990.

Favier, L., Durand, G., Cornford, S. L., Gudmundsson, G. H., Gagliardini, O., Gillet-Chaulet, F., Zwinger, T., Payne, A. J., and Brocq, A. M. L.: Retreat of Pine Island Glacier controlled by marine ice-sheet instability, Nature Climate Change, 4, 117–121, https://doi.org/10.1038/nclimate2094, 2014.

Fretwell, P., Pritchard, H. D., Vaughan, D. G., Bamber, J. L., Barrand, N. E., Bell, R., Bianchi, C., Bingham, R. G., Blankenship, D. D., Casassa, G., Catania, G., Callens, D., Conway, H., Cook, A. J., Corr, H. F., Damaske, D., Damm, V., Ferraccioli, F., Forsberg, R., Fujita, S., Gim, Y., Gogineni, P., Griggs, J. A., Hindmarsh, R. C., Holmlund, P., Holt, J. W., Jacobel, R. W., Jenkins, A., Jokat, W., Jordan, T., King, E. C., Kohler, J., Krabill, W., Riger-Kusk, M., Langley, K. A., Leitchenkov, G., Leuschen, C., Luyendyk, B. P., Matsuoka, K., Mouginot, J., Nitsche, F. O., Nogi, Y., Nost, O. A., Popov, S. V., Rignot, E., Rippin, D. M., Rivera, A., Roberts, J., Ross, N., Siegert, M. J., Smith, A. M., Steinhage, D., Studinger, M., Sun, B., Tinto, B. K., Welch, B. C., Wilson, D., Young, D. A., Xiangbin, C., and Zirizzotti, A.: Bedmap2: Improved ice bed, surface and thickness datasets for Antarctica, Cryosphere, 7, 375–393, https://doi.org/10.5194/tc-7-375-2013, 2013.

Fricker, H. A., Scambos, T., Bindschadler, R., and Padman, L.: An Active Subglacial Water System in West Antarctica Mapped from Space, Science, 315, 1544–1548, https://doi.org/10.1126/science.1136897, 2007.

Gagliardini, O., Cohen, D., Råback, P., and Zwinger, T.: Finite-element modeling of subglacial cavities and related friction law, Journal of Geophysical Research: Earth Surface, 112, https://doi.org/10.1029/2006JF000576, 2007.

Gillet-Chaulet, F., Durand, G., Gagliardini, O., Mosbeux, C., Mouginot, J., Rémy, F., and Ritz, C.: Assimilation of surface velocities acquired between 1996 and 2010 to constrain the form of the basal friction law under Pine Island Glacier, Geophysical Research Letters, 43, 10,311–10,321, https://doi.org/10.1002/2016GL069937, 2016.

Gladstone, R. M., Warner, R. C., Galton-Fenzi, B. K., Gagliardini, O., Zwinger, T., and Greve, R.: Marine ice sheet model performance depends on basal sliding physics and sub-shelf melting, Cryosphere, 11, 319–329, https://doi.org/10.5194/tc-11-319-2017, 2017.

Graham, A. G., Wåhlin, A., Hogan, K. A., Nitsche, F. O., Heywood, K. J., Totten, R. L., Smith, J. A., Hillenbrand, C. D., Simkins, L. M., Anderson, J. B., Wellner, J. S., and Larter, R. D.: Rapid retreat of Thwaites Glacier in the pre-satellite era, Nature Geoscience, 15, 706–713, https://doi.org/10.1038/s41561-022-01019-9, 2022.

Granick, S.: Soft matter in a tight spot, Physics Today, 52, 26–31, https://doi.org/10.1063/1.882747, 1999.

Gray, L., Joughin, I., Tulaczyk, S., Spikes, V. B., Bindschadler, R., and Jezek, K.: Evidence for subglacial water transport in the West Antarctic Ice Sheet through three-dimensional satellite radar interferometry, Geophysical Research Letters, 32, 1–4, https://doi.org/10.1029/2004GL021387, 2005.

https://doi.org/10.5194/egusphere-2025-764
Preprint. Discussion started: 17 March 2025

Gudmundsson, G. H., Paolo, F. S., Adusumilli, S., and Fricker, H. A.: Instantaneous Antarctic ice sheet mass loss driven by thinning ice shelves, Geophysical Research Letters, 46, 13 903–13 909, https://doi.org/https://doi.org/10.1029/2019GL085027, 2019.

Hank, K. and Tarasov, L.: The comparative role of physical system processes in Hudson Strait ice stream cycling: a comprehensive model-based test of Heinrich event hypotheses, Climate of the Past, 20, 2499–2524, https://doi.org/10.5194/cp-20-2499-2024, 2024.

Hoffman, M. J., Perego, M., Price, S. F., Lipscomb, W. H., Zhang, T., Jacobsen, D., Tezaur, I., Salinger, A. G., Tuminaro, R., and Bertagna, L.: MPAS-Albany Land Ice (MALI): a variable-resolution ice sheet model for Earth system modeling using Voronoi grids, Geoscientific Model Development, 11, 3747–3780, https://doi.org/10.5194/gmd-11-3747-2018, 2018.

Iken, A.: The Effect of the Subglacial Water Pressure on the Sliding Velocity of a Glacier in an Idealized Numerical Model, Journal of Glaciology, 27, 407–421, https://doi.org/10.3189/s0022143000011448, 1981.

IPCC Core Writing Team, H. Lee and J. Romero (eds.): IPCC 2023: Summary for Policymakers. In: Climate Change 2023: Synthesis Report. Contribution of Working Groups I, II and III to the Sixth Assessment Report of the Intergovernmental Panel on Climate Change, IPCC, Geneva, Switzerland, https://doi.org/10.59327/IPCC/AR6-9789291691647.001, 2023.

Israelachvili, J. N.: Measurements of the viscosity of thin fluid films between two surfaces with and without adsorbed polymers, 1986.

Iverson, N. R.: Shear resistance and continuity of subglacial till: Hydrology rules, https://doi.org/10.3189/002214311796406220, 2010.

Iverson, N. R., Hoover, T. S., and Baker, R. W.: Ring-shear studies of till deformation: Coulomb-plastic behavior and distributed strain in glacier beds, Journal of Glaciology, 44, 634–642, https://doi.org/10.1017/S0022143000002136, 1998.

Joughin, I., Smith, B. E., and Schoof, C. G.: Regularized Coulomb Friction Laws for Ice Sheet Sliding: Application to Pine Island Glacier, Antarctica, Geophysical Research Letters, 46, 4764–4771, https://doi.org/10.1029/2019GL082526, 2019.

Kirshner, A. E., Anderson, J. B., Jakobsson, M., O'Regan, M., Majewski, W., and Nitsche, F. O.: Post-LGM deglaciation in Pine Island Bay, West Antarctica, Quaternary Science Reviews, 38, 11–26, https://doi.org/10.1016/j.quascirev.2012.01.017, 2012.

Kyrke-Smith, T. M., Gudmundsson, G. H., and Farrell, P. E.: Can Seismic Observations of Bed Conditions on Ice Streams Help Constrain Parameters in Ice Flow Models?, Journal of Geophysical Research: Earth Surface, 122, 2269–2282, https://doi.org/10.1002/2017JF004373, 2017.

Larour, E., Schiermeier, J., Rignot, E., Seroussi, H., Morlighem, M., and Paden, J.: Sensitivity Analysis of Pine Island Glacier ice flow using ISSM and DAKOTA, Journal of Geophysical Research: Earth Surface, 117, https://doi.org/10.1029/2011JF002146, 2012.

Lee, K. M., Ballard, M. S., McNeese, A. R., Muir, T. G., Wilson, P. S., Costley, R. D., and Hathaway, K. K.: In situ measurements of sediment acoustic properties in Currituck Sound and comparison to models, The Journal of the Acoustical Society of America, 140, 3593–3606, https://doi.org/10.1121/1.4966118, 2016.

Lliboutry, L.: Contribution à la théorie du frottement du glacier sur son lit, CR Hebd. Séances Acad. Sci, 247, 318–320, 1958a.

Lliboutry, L.: Frottement sur le lit et mouvement par saccades d'un glacier, CR Hebd. Seances Acad. Sci, 247, 228–230, 1958b.

Lliboutry, L.: Une théorie du frottement du glacier sur son lit, in: Annales de Géophysique, vol. 15, p. 250, 1959.

Luengo, G., Lsraelachvili, J., and Granick, S.: Generalized effects in confined fluids: new friction map for boundary lubrication, 1996.

Lüthi, M., Funk, M., Iken, A., Gogineni, S., and Truffer, M.: Mechanisms of fast flow in Jakobshavn Isbræ, West Greenland: Part III. Measurements of ice deformation, temperature and cross-borehole conductivity in boreholes to the bedrock, Journal of Glaciology, 48, 369–385, https://doi.org/10.3189/172756502781831322, 2002.

Mouginot, J., Scheuchl, B., and Rignot., E.: MEaSUREs Annual Antarctic Ice Velocity Maps 2005-2017, Version 1. 2014/5]., https://doi.org/10.5067/9T4EPQXTJYW9, 2022.

https://doi.org/10.5194/egusphere-2025-764
Preprint. Discussion started: 17 March 2025

Muto, A., Peters, L. E., Gohl, K., Sasgen, I., Alley, R. B., Anandakrishnan, S., and Riverman, K. L.: Subglacial bathymetry and sediment distribution beneath Pine Island Glacier ice shelf modeled using aerogravity and in situ geophysical data: New results, Earth and Planetary Science Letters, 433, 63–75, https://doi.org/https://doi.org/10.1016/j.epsl.2015.10.037, 2016.

Nias, I. J., Cornford, S. L., and Payne, A. J.: New Mass-Conserving Bedrock Topography for Pine Island Glacier Impacts Simulated Decadal Rates of Mass Loss, Geophysical Research Letters, 45, 3173–3181, https://doi.org/https://doi.org/10.1002/2017GL076493, 2018.

Ranganathan, M., Minchew, B., Meyer, C. R., and Gudmundsson, G. H.: A new approach to inferring basal drag and ice rheology in ice streams, with applications to West Antarctic Ice Streams, Journal of Glaciology, 67, 229–242, https://doi.org/10.1017/jog.2020.95, 2021.

Richardson, M. D., Briggs, K. B., Bibee, L. D., Jumars, P. A., Sawyer, W. B., Albert, D. B., Bennett, R. H., Berger, T. K., Buckingham, M. J., Chotiros, N. P., Dahl, P. H., Dewitt, N. T., Fleischer, P., Flood, R., Greenlaw, C. F., Holliday, D. V., Hulbert, M. H., Hutnak, M. P., Jackson, P. D., Jaffe, J. S., Johnson, H. P., Lavoie, D. L., Lyons, A. P., Martens, C. S., Mcgehee, D. E., Moore, K. D., Orsi, T. H., Piper, J. N., Ray, R. I., Reed, A. H., Self, R. F. L., Schmidt, J. L., Schock, S. G., Simonet, F., Stoll, R. D., Tang, D., Thistle, D. E., Thorsos, E. I., Walter, D. J., Wheatcroft, R. A., Richardson, M. D., Briggs, K. B., Bibee, L. D., Sawyer, W. B., Lavoie, D. L., Ray, R. I., Reed, A. H., Walter, D. J., Jumars, P. A., Albert, D. B., Martens, C. S., Buckingham, M. J., Dahl, P. H., Tang, D., and Thorsos, E. I.: Overview of SAX99: Environmental Considerations, 2001.

Ritz, C., Edwards, T. L., Durand, G., Payne, A. J., Peyaud, V., and Hindmarsh, R. C.: Potential sea-level rise from Antarctic ice-sheet instability constrained by observations, Nature, 528, 115–118, https://doi.org/10.1038/nature16147, 2015.

Savage, W., Morrissey, M., and andRL Baum: Geotechnical Properties for Landslide-Prone Seattle Area Glacial Deposits, U.S. Geological Survey, 2000.

Schoof, C.: The effect of cavitation on glacier sliding, Proceedings of the Royal Society A: Mathematical, Physical and Engineering Sciences, 461, 609–627, https://doi.org/10.1098/rspa.2004.1350, 2005.

Smith, A. M., Jordan, T. A., Ferraccioli, F., and Bingham, R. G.: Influence of subglacial conditions on ice stream dynamics: Seismic and potential field data from Pine Island Glacier, West Antarctica, Journal of Geophysical Research: Solid Earth, 118, 1471–1482, https://doi.org/https://doi.org/10.1029/2012JB009582, 2013.

Smith, A. M., Anker, P. G. D., Nicholls, K. W., Makinson, K., Murray, T., Rios-Costas, S., Brisbourne, A. M., Hodgson, D. A., Schlegel, R., and Anandakrishnan, S.: Ice stream subglacial access for ice-sheet history and fast ice flow: the BEAMISH Project on Rutford Ice Stream, West Antarctica and initial results on basal conditions, Annals of Glaciology, 62, 203–211, https://doi.org/10.1017/aog.2020.82, 2021.

Smith, B., Fricker, H. A., Gardner, A. S., Medley, B., Nilsson, J., Paolo, F. S., Holschuh, N., Adusumilli, S., Brunt, K., Csatho, B., Harbeck, K., Markus, T., Neumann, T., R, S. M., and Zwally, H. J.: Pervasive ice sheet mass loss reflects competing ocean and atmosphere processes, Science, 368, 1239–1242, contains maps of thinning rates in Antarctica, demonstrating the significant thinning of WAIS over the satellite period., 2020.

Smith, B. E., Fricker, H. A., Joughin, I. R., and Tulaczyk, S.: An inventory of active subglacial lakes in Antarctica detected by ICESat (2003-2008, Journal of Glaciology, 55, 573–595, https://doi.org/10.3189/002214309789470879, 2009.

Smith, J. A., Hillenbrand, C.-D., Kuhn, G., Larter, R. D., Graham, A. G., Ehrmann, W., Moreton, S. G., and Forwick, M.: Deglacial history of the West Antarctic Ice Sheet in the western Amundsen Sea Embayment, Quaternary Science Reviews, 30, 488–505, https://doi.org/https://doi.org/10.1016/j.quascirev.2010.11.020, 2011.

Smith, J. A., Hillenbrand, C. D., Kuhn, G., Klages, J. P., Graham, A. G., Larter, R. D., Ehrmann, W., Moreton, S. G., Wiers, S., and Frederichs, T.: New constraints on the timing of West Antarctic Ice Sheet retreat in the eastern Amundsen Sea since the Last Glacial Maximum, Global and Planetary Change, 122, 224–237, https://doi.org/10.1016/j.gloplacha.2014.07.015, 2014.

https://doi.org/10.5194/egusphere-2025-764
Preprint. Discussion started: 17 March 2025

Smith, J. A., Andersen, T. J., Shortt, M., Gaffney, A. M., Truffer, M., Stanton, T. P., Bindschadler, R., Dutrieux, P., Jenkins, A., Hillenbrand, C. D., Ehrmann, W., Corr, H. F., Farley, N., Crowhurst, S., and Vaughan, D. G.: Sub-ice-shelf sediments record history of twentieth-century retreat of Pine Island Glacier, Nature, 541, 77–80, https://doi.org/10.1038/nature20136, 2017.

Stone, D. B. and Clarke, G. K.: Estimation of subglacial hydraulic properties from induced changes in basal water pressure: a theoretical framework for borehole-response tests, Journal of Glaciology, 39, 327–340, https://doi.org/10.3189/s0022143000015999, 1993.

Tsai, V. C., Stewart, A. L., and Thompson, A. F.: Marine ice-sheet profiles and stability under Coulomb basal conditions, Journal of Glaciology, 61, 205–215, https://doi.org/10.3189/2015JoG14J221, 2015.

Tulaczyk, S., Kamb, W. B., and Engelhardt, H. F.: Basal mechanics of Ice Stream B, West Antarctica 1. Till mechanics, Journal of Geophysical Research: Solid Earth, 105, 463–481, https://doi.org/10.1029/1999jb900329, 2000.

Weertman, J.: On the Sliding of Glaciers, Journal of Glaciology, 3, 33–38, https://doi.org/10.3189/s0022143000024709, 1957.

Yamada, S.: Layering transitions and tribology of molecularly thin films of poly(dimethylsiloxane), Langmuir, 19, 7399–7405, https://doi.org/10.1021/la0345111, 2003.

Zoet, L. K. and Iverson, N. R.: A slip law for glaciers on deformable beds, Science, 368, https://doi.org/10.1126/science.aaz1183, 2020.